Meas. Sci. Technol. **20** (2009) 015401 (11pp) doi:10.1088/0957-0233/20/1/015401

Two-color laser-induced fluorescent thermometry for microfluidic systems

V K Natrajan and K T Christensen

Department of Mechanical Science and Engineering, University of Illinois, Urbana, IL 61801, USA

E-mail: ktc@illinois.edu

Received 19 August 2008, in final form 13 October 2008
Published 12 November 2008
Online at stacks.iop.org/MST/20/015401

Abstract

The feasibility of implementing a two-color laser-induced fluorescence (LIF) technique to study thermal transport at the microscale is investigated. Temperature-sensitive (Rhodamine B) and temperature-insensitive (Sulforhodamine-101) fluorescent dyes are used in tandem to determine fluid temperature with high accuracy and low noise using a pulsed Nd:YAG laser as an illumination source. While the fluorescence intensity of the temperature-sensitive dye is proportional to temperature, it is also biased by variations in the illuminating intensity. Therefore, a second temperature-insensitive dye is required to compensate for such biases. Calibration of the two-color LIF system using the RhB–SR101 dye combination in ethanol and water yields temperature sensitivities of $-1.5\%\ \mathrm{K}^{-1}$ and $-2.7\%\ \mathrm{K}^{-1}$, respectively, with volumetric illumination from an Nd:YAG laser. The feasibility of this methodology for conducting temperature measurements is explored by measuring a steady-state temperature gradient maintained across a microfluidic channel array by two large hot and cold reservoirs. These measurements reveal that the mean steady-state temperatures in the microchannels are within $\pm 0.4\,^{\circ}\mathrm{C}$ and $\pm 0.3\,^{\circ}\mathrm{C}$ of the predicted temperatures with ethanol and water as the solvents, respectively, with a spatial resolution of $22.2 \times 22.2\ \mu\mathrm{m}$. The experimental uncertainties in the measurements using the RhB–SR101 dye combination are ± 0.48–$0.59\,^{\circ}\mathrm{C}$ and ± 0.41–$0.49\,^{\circ}\mathrm{C}$ for ethanol and water, respectively.

Keywords: temperature, laser-induced fluorescence, microfluidics

1. Introduction

The recent development of microfluidic systems such as μ-total-analysis systems (μ-TAS) and μ-heat exchangers have led to a growing demand for the development of precision microscale measurement techniques to monitor both momentum and thermal transport. In such devices, the accurate assessment of temperature will not only aid in the optimization of their design, but will also maximize their efficiency, reliability and productivity during operation [1]. For instance, precision control of fluid temperature by accounting for local temperature gradients could optimize chemical operations such as mixing, reactions and separations within complex microfluidic systems, including lab-on-a-chip devices or microscale fuel cells [2, 3]. Such control becomes crucial when electrokinetic pumping is used for driving flow through these devices as the current flowing through the buffer solution can result in significant internal heat generation, a phenomenon known as Joule heating [4]. Since most microfluidic-based microelectromechanical systems (MEMS) utilize very high heat and mass transfer rates, a thorough understanding of their thermal transport characteristics is paramount for optimizing their design for increased performance and reliability.

While several methods exist for measurement of fluid temperature at the macroscale, the direct applications of these methods to the microscale may not be possible. In particular, accurate determination of temperature gradients is extremely challenging at the microscale because dissipation of such gradients occurs over very short timescales due to high heat-transfer rates. Therefore, while several techniques exist for measurement of temperature at the macroscale, where the limiting factors of thermal transport are not as severe, methods with similar accuracy at the microscale are only now being

pursued. Most temperature measurements in microfluidic systems were limited to, until recently, measurements of bulk fluid temperature at the inlet and outlet of microfluidic sections or measurements of the substrate's temperature itself. With regard to local temperature measurements, the use of high-precision thermocouple probes to measure fluid and/or substrate temperature is generally restrictive. In addition to being intrusive, these probes can suffer from poor spatial and temporal resolution since most probes have a characteristic size comparable to that of the microchannels under consideration. Alternatively, microfluidic devices can also be fabricated with integrated resistance temperature detectors (RTDs) embedded in the substrate with spatial extents on the order of a few microns [5]. However, the fabrication procedure for RTDs is often quite complex and they suffer from poor spatial resolution which limits their ability to resolve local temperature gradients. Further, while these sensors are convenient for monitoring surface temperature, they do not provide a direct measure of the local fluid temperature.

One of the most accurate temperature-measurement methods at the macroscale is laser-induced fluorescence (LIF). In this technique, a temperature-sensitive fluorescent dye is dissolved within the fluid of interest and the dye is excited to fluoresce with an illumination source [6]. The local intensity of the fluoresced light is proportional to the local temperature of the fluid but with a limited accuracy of roughly $\pm 2.0\,^{\circ}\mathrm{C}$, primarily due to variations in the intensity of the illumination source. To overcome such issues, Sakakibara and Adrian [7] introduced a second dye into the solution whose fluorescence intensity was temperature-insensitive, yielding a local measure of incident intensity variations within their continuous illumination source. The fluoresced light from each dye was imaged by separate cameras and the ratio of these intensities led to an estimate of temperature with a much-improved accuracy of $\pm 0.2\,^{\circ}\mathrm{C}$ [8, 9]. In contrast, Lavieille *et al* [10] utilized a single-dye, two-color technique wherein variations in dye concentration and illumination intensity were reduced by computing the intensity ratio of the temperature-dependent and temperature-independent portions of the emission from Rhodamine B at higher and lower wavelengths, respectively. More recently, as an extension of their previous work, Bruchhausen *et al* [11] demonstrated the efficacy of this single-dye methodology by performing instantaneous measurements of fluid temperature at the macroscale using a pulsed Nd:YAG laser for illumination and by taking into account the reabsorption of the fluorescence emission by the medium itself.

There are two main impediments associated with successfully implementing LIF methods at the microscale. First, most microfluidic systems, like lab-on-a-chip devices, generally only allow optical access from the top of the device (along the z direction if the channel network lies in the x–y plane). Therefore, one is forced to illuminate the test section from the z-direction which will inherently illuminate the entire depth dimension of the domain of interest. As has been observed extensively in microscopic particle image velocimetry (PIV) applications, volume illumination significantly increases the out-of-focus noise levels. Ross *et al* [12] attempted LIF temperature measurements via volume illumination with a continuous light source and a single temperature-sensitive dye in a microfluidic device and their system yielded a measurement accuracy of $\pm 1.5\,^{\circ}\mathrm{C}$. However, it is not clear whether this limited accuracy was associated with the adverse effects of volume illumination, variations in illumination intensity, or both. Alternatively, one can employ a continuous micro-lasersheet ($\sim$10 μm thickness) as an illumination source. Yoon and Kim [13] designed a special microchannel with optical access from both the side and above and employed such a device for illumination of a much thinner region in the depth dimension for measurements of concentration fields by LIF. This methodology reduced the out-of-plane noise significantly, although it cannot be easily applied to complex channel networks. Further, temperature was not inferred from these LIF measurements, so it is not clear whether any improvements might be garnered with such an illumination methodology.

The second difficulty encountered in measurement of temperature at the microscale involves the thermal-transport timescales. Given that the timescale of heat dissipation at the microscale is quite short, coupled with the fact that the intensity of the incident light must be high enough to yield measurable fluorescence from the dyes, continuous illumination via an Argon laser (the standard for LIF at the macroscale) nor the aforementioned micro-lasersheet employed by Yoon and Kim [13] are likely not appropriate. However, pulsed lasers, such as the Nd:YAG laser, can provide sufficient illumination intensity over timescales much shorter than those of thermal transport at the microscale, meaning instantaneous measurements of temperature may be possible [11].

To this end, a two-dye LIF methodology is under development to allow accurate measurements of instantaneous fluid temperature at the microscale. Although the two-dye methodology has been previously adapted to the microscale by Kim *et al* [14], these experiments were performed using a continuous Argon laser as an illumination source with a combination of Rhodamine B and Rhodamine 110 dyes. In addition, these experiments utilized a single camera and relied upon temporal switching of filters upstream of the camera to image the fluorescence from the dyes. While this imaging arrangement avoids registration errors associated with a two-camera system, instantaneous measurement of temperature via two-dye LIF with a single camera is not possible since the fluorescent emissions of the two dyes cannot be acquired simultaneously. Further, the LIF parameters of Kim *et al* [14] are identical to the experimental protocols commonly used at the macroscale where the thermal timescales are quite long. However, as outlined above, given the short timescales involved in thermal transport at the microscale, use of a continuous illumination source can severely limit the accuracy of temperature measurements at these scales. The current study assesses the feasibility of applying the two-dye LIF methodology at the microscale using a pulsed Nd:YAG laser emitting in the green (second-harmonic emission) as the illumination source. As with previous micro- and macro-scale studies, Rhodamine B is utilized as the temperature-sensitive

dye since its absorption spectrum overlaps the second-harmonic emission wavelength of the Nd:YAG. In contrast, Rhodamine 110 cannot be used as the temperature-insensitive dye since its absorption spectrum resides predominantly below the second-harmonic emission of the Nd:YAG laser. An alternative fluorescent dye is proposed that accounts for variations in incident illumination intensity and its spectral and temperature-dependent characteristics are documented. The suitability of the alternative dye for temperature measurements using the two-color LIF technique is also assessed. By accounting for variations in illumination intensity, this study provides a measure of how detrimental volume illumination effects can be in microscale implementations of fluorescent thermometry.

2. Principles of LIF

When a photon of given energy is absorbed by a fluorophore, the energy state of the molecule transitions from the ground state to higher electronic states. Energy is subsequently dissipated at these excited states until the molecule reaches the lowest level of the first excited singlet state. Thereafter, the molecule at the first singlet state can return to the ground state in multiple ways. One such path of return is via fluorescence, defined as a radioactive decay process wherein no further energy is dissipated by collisions and the return of the excited molecule to the ground state occurs purely by the emission of energy. In such a scenario, a portion of the remaining energy is lost by the molecule before the emission and consequently, the emitted energy is of longer wavelength than the energy it initially absorbed. This shift in the wavelength of the fluoresced light relative to the absorption wavelength is referred to as the Stokes shift.

For a dye of concentration C (kg m^{-3}) illuminated with an incident light flux of intensity $I_\circ$ (W m^{-3}), the fluorescence energy emitted per unit volume, I (W m^{-3}), is

$$I = I_\circ C \phi \varepsilon, \tag{1}$$

where ε is the absorption coefficient of the dye and ϕ is its quantum efficiency. For most organic dyes, variations in I with temperature are predominantly attributable to the temperature dependence of the quantum efficiency though, for some dyes, the absorption coefficient can also depend on temperature. Therefore, in principle, if one can maintain $I_\circ$ and C constant, the temperature of a fluorescent dye solution can be measured through variations of fluorescence intensity associated with the temperature dependence of the product $\phi\varepsilon$. However, while maintaining a constant concentration is certainly achievable, it is impossible to maintain a constant incident light flux. Therefore, the fluorescence intensity not only embodies variations in solution temperature but also variations in the illumination intensity. Hence, the accuracy of fluid-temperature measurement with a single fluorescent dye is inherently limited by the homogeneity and stability of the illumination technique employed.

In order to alleviate accuracy limitations associated with variations in the illumination intensity, a second fluorescent dye, whose quantum efficiency and absorption coefficient have little, or no, temperature dependence is added to the solution and the fluorescence intensity of the two dyes is imaged simultaneously. Therefore, while the intensity of the fluoresced light from the temperature-dependent dye embodies both variations in temperature and illuminating intensity, any variations in the fluorescence intensity of the temperature-insensitive dye are directly attributable to variations in the illuminating intensity. If the emission from the two dyes, labeled A (temperature sensitive) and B (temperature insensitive), are separated perfectly into cameras α and β, respectively, the ratio of the fluorescence intensities recorded by both cameras is expressed as

$$\frac{V^\alpha}{V^\beta} = \frac{I_A}{I_B} = \frac{C_A \phi_A \varepsilon_A}{C_B \phi_B \varepsilon_B} \neq f(I_\circ), \tag{2}$$

where V^α and V^β are voltage outputs from the CCDs of cameras α and β, respectively. This ratio is independent of the incident light flux $I_\circ$ but depends on temperature via the ratio $\phi_A\varepsilon_A/\phi_B\varepsilon_B$. In practice, however, it is impossible to completely separate I_A and I_B, both because the emission spectra of most organic dyes are rather broad, meaning some overlap of their emissions is to be expected, and because spectral filters are inherently imperfect (filtering efficiencies of 90–95% are typical). For the case of imperfect separation of the emission of two fluorescent dyes, wherein some fraction of the emission from dyes A and B are imaged by cameras β and α, respectively, the expression

$$\frac{V^\alpha}{V^\beta} = \frac{I_A + \Pi_B I_B}{I_B + \Pi_A I_A} \neq f(I_\circ) \tag{3}$$

accounts for this effect [8]. Here $\Pi_A = V^\beta_{C_B=0}/V^\alpha_{C_B=0}$ represents the ratio of the emission from dye A imaged by cameras β and α, respectively, with $C_B = 0$, and $\Pi_B = V^\alpha_{C_A=0}/V^\beta_{C_A=0}$ represents the ratio of the emission from dye B imaged by cameras α and β, respectively, with $C_A = 0$. In this context, $V^\alpha_{C_A=0}$, $V^\alpha_{C_B=0}$, $V^\beta_{C_A=0}$ and $V^\beta_{C_B=0}$ are constants for a given optical configuration. As with the case of perfect separation, the ratio in equation (3) is independent of the illumination intensity, $I_\circ$, and is therefore only a function of the fluid temperature, T.

3. Experimental setup

Figure 1 presents a detailed schematic of a typical experimental setup used for imaging the emission of the two dyes in a microfluidic device of interest. This setup is essentially identical to that commonly utilized in microscopic PIV save for an additional camera and additional filters. Light from an Nd:YAG laser ($\lambda = 532$ nm, 12 mJ, Continuum) is navigated through a microscope (Olympus BX60) to illuminate the test section. The fluorescence emission from the dyes passes through a 10× objective lens (Olympus UPlan Fl: numerical aperture: 0.30, working distance: 10.0 mm, depth of field: 14.72 μm) followed by a dichroic filter cube ($\lambda > 550$ nm, Chroma Filter) that suppresses all remaining incident light but passes the higher-wavelength emissions of the dyes. The light fluoresced by each dye is then separated using a second dichroic filter cube ($\lambda = 600$ nm, Chroma Filter) that reflects

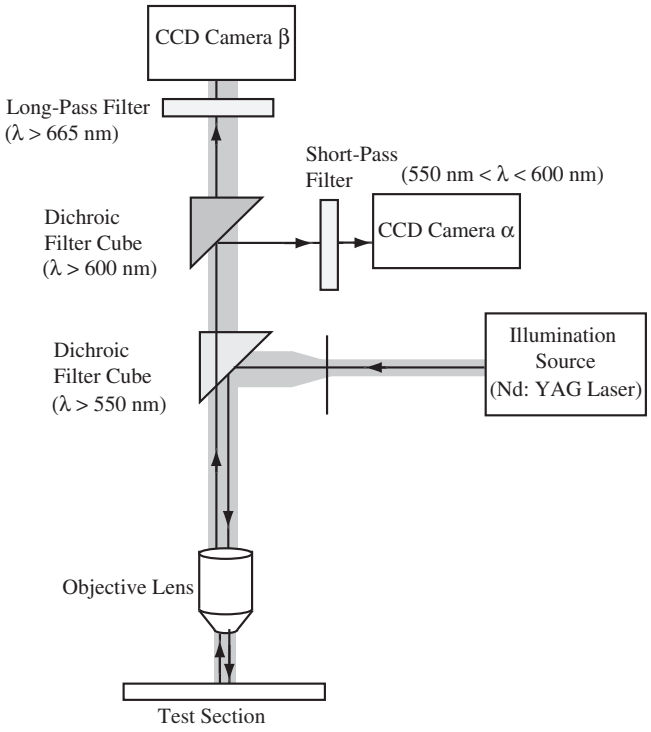

Figure 1. Schematic of the experimental arrangement for two-color LIF at the microscale.

wavelengths of $\lambda < 600$ nm toward camera α and transmits higher wavelengths toward camera β. A narrow band-pass filter (550 nm $< \lambda <$ 580 nm, Melles Griot) just upstream of camera α provides an additional filtering step before the fluoresced light is imaged. Similarly, an additional long-pass filter ($\lambda >$ 665 nm, Melles Griot) is positioned just upstream of camera β to further purify this fluoresced light prior to imaging. The cameras utilized in this effort are identical 12-bit, cooled CCD cameras with an effective chip area of 1396 × 1040 pixels (Photometric, CoolSnap HQ2) and are attached to the microscope using a dual-camera attachment (U-DPTS, Olympus) which maintains the same focal plane in both cameras. Precise synchronization between the firing of the laser pulses and the acquisition of images by both cameras is achieved with a digital delay generator (Model 500 Pulse Generator, BNC). In this arrangement, the imaging system has a spatial resolution of 0.74 μm pixel^{-1}.

While the two-camera adapter employed herein ensures that cameras α and β maintain the same focal plane and therefore have identical magnifications, the image of one camera relative to the other will inevitably have some rotational and translational differences due to slight discrepancies in the orientation of each CCD array relative to its camera housing, etc. These differences are exacerbated significantly when imaging over sub-millimeter fields of view and must therefore be accounted for since the two-dye methodology under consideration requires one to divide the two intensity fields, pixel-by-pixel as outlined in equation (2), to determine the temperature distribution over the spatial domain of interest. In order to register the images acquired by cameras α and β relative to one-another, a mapping function must be determined by calibrating the image coordinates of each camera using a suitable target so that a one-to-one correspondence is obtained between each pixel location in the two CCD arrays. This procedure ensures that the pairs of pixels identified from the two CCD arrays using the mapping function revert back to the same physical coordinates in the measurement plane. It is important to note that since the magnification of the images acquired by both cameras is identical and does not vary across the image field, the mapping function utilized herein is simply a geometric one. However, in experiments where image distortion cannot be avoided resulting in variable magnification across the images, one must account for these registration errors using a more complex mapping methodology like those often employed in stereoscopic PIV [15].

The geometric mapping methodology employed herein is illustrated in figure 2(a) which presents images A and B of a sample target, acquired simultaneously, using cameras α and β, respectively. The image coordinates are registered relative to one-another by first determining the relative rotation between the images. Once this relative rotation is accounted for in image B (yielding image B′), a spatial cross-correlation is performed between images A and B′ to determine the relative horizontal and vertical translations of image B′ with respect to image A. Figure 2(b) presents the final result of this mapping methodology applied to the calibration images in figure 2(a) and reveals quite good spatial correspondence between the pixel locations in both CCD arrays. In this regard, the spatial uncertainty of this mapping procedure is estimated to be approximately 7×7 pixels which corresponds to 5.2×5.2 μm in physical units.

4. Fluorescent dye selection

There are several important factors that must be considered in the selection of appropriate dyes for a two-dye LIF system. First, the combination of a temperature-insensitive dye and a strong temperature-dependent dye is preferred since it will maximize the temperature sensitivity of the ratio of the fluorescence emissions from dyes A and B, respectively. In addition, since the dyes are excited by a single illumination source, they should have similar absorption characteristics yet quite different emission spectra. The latter requirement is crucial for efficient optical separation before imaging. Finally, the dyes must be efficiently dissolved in the solution and well-mixed at the molecular level for accurate measurements of the intensity ratio at the microscale.

Rhodamine B (RhB) is chosen as the temperature-sensitive dye for the present effort. This dye is soluble in water as well as organic solvents like ethanol and displays a rather strong temperature sensitivity (-2.6% K^{-1} and -1.45% K^{-1} when dissolved in water and ethanol, respectively). In addition, RhB absorbs light at $\lambda_{abs} \approx 535$ nm and fluoresces over a wavelength range of 525 nm $\lesssim \lambda_{em} \lesssim$ 580 nm when dissolved in either water or ethanol [10]. These characteristics are quite advantageous in the present effort because the dye can be easily excited by an Nd:YAG laser emitting in the green while a portion of its fluorescence

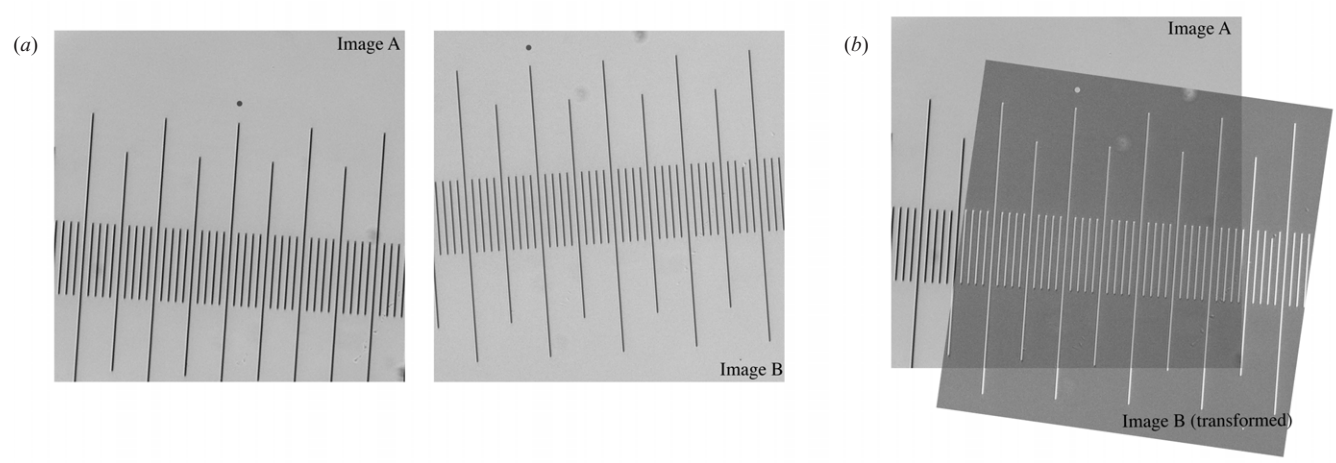

Figure 2. (a) Images of a target acquired simultaneously with cameras α and β, respectively, used to register the cameras relative to one-another. (b) Result of applying a transformation to image B via a geometric mapping function.

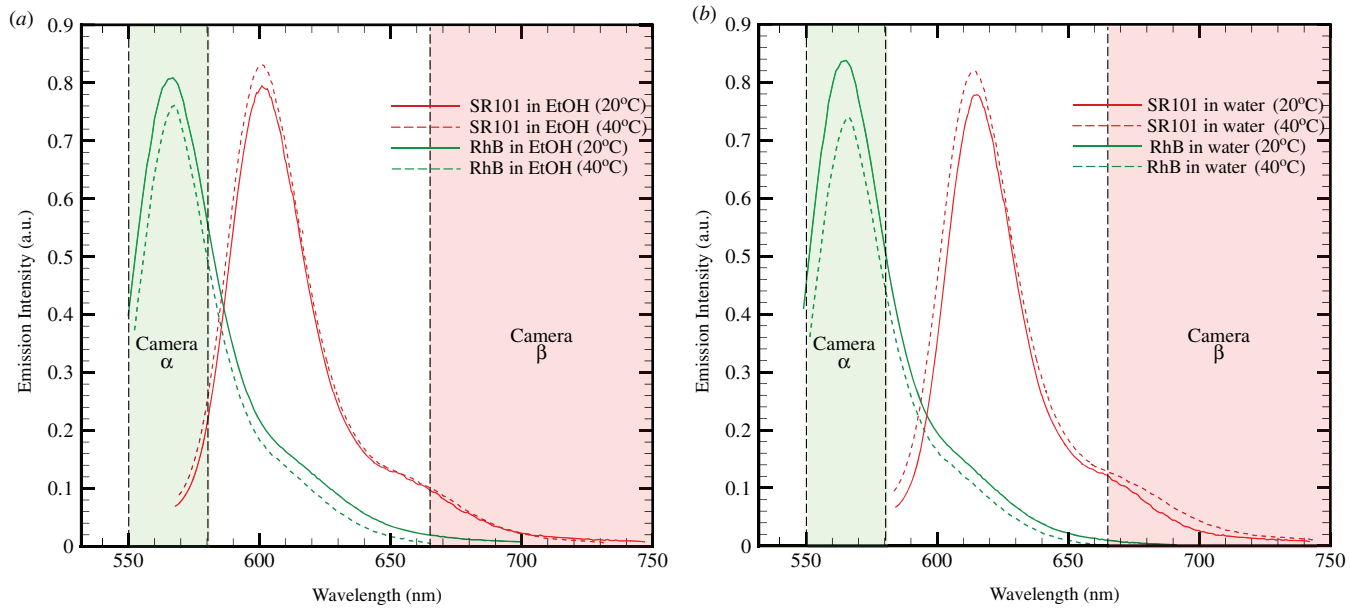

Figure 3. Emission spectra of RhB and SR101 dissolved in (a) ethanol and (b) water at 20 °C and 40 °C when excited at 532 nm. The shaded regions demarcate the wavelengths that are imaged by cameras α and β in the experimental arrangement presented in figure 1.

occurs at higher wavelengths, facilitating efficient separation of the emission wavelength from the illuminating wavelength. Sulforhodamine-101 (SR101) is selected as the second dye because of the large Stokes shift that it exhibits [16]. Its absorption spectrum is suitable for excitation using an Nd:YAG laser in the green ($\lambda_{abs} \approx 558$ nm and 550 nm in ethanol and water, respectively) and its emission spectrum ($\lambda_{em} \approx 610$ nm and 620 nm in ethanol and water, respectively) can be separated from both the illuminating wavelength and the emission wavelength of RhB when dissolved in either ethanol or water. Additionally, the fluorescence intensity of SR101 increases slightly with increasing temperature [16], in stark contrast to the temperature dependence exhibited by RhB. As such, the temperature sensitivity of the RhB–SR101 combination is actually higher than that achievable with RhB in concert with a dye with no sensitivity to temperature.

Figures 3(a) and 3(b) present the emission spectra of both dyes when dissolved in ethanol and water, respectively, at 20 °C and 40 °C, when excited at 532 nm. Note that the emission characteristics of both dyes are excluded for $\lambda < 550$ nm since the optical arrangement utilized herein blocks these wavelengths prior to imaging to ensure suppression of all remaining illumination light. The shaded regions in figures 3(a) and 3(b) highlight the wavelengths of light transmitted by the low-pass (550 nm $< \lambda <$ 580 nm) and the high-pass ($\lambda >$ 665 nm) filters prior to imaging by cameras α and β, respectively. When dissolved in ethanol (figure 3(a)), both dyes have broad emission spectra with overlapping wavelengths in the range 570 nm $< \lambda <$ 660 nm, with their emission peaks separated by 40 nm. On the other hand, with water as the solvent (figure 3(b)), the emission spectra of both dyes overlap in the wavelength range 590 nm $< \lambda <$ 650 nm, and their emission peaks are separated by 50 nm. Figures 3(a)

and 3(b) illustrate that the emission intensity of RhB dissolved either in water or ethanol decreases over all wavelengths presented when the temperature of the dye is raised from 20 °C to 40 °C. (Again, as noted earlier, the temperature dependence of the emission intensity of RhB is a strong function of wavelength in the range 525 nm $\lesssim \lambda \lesssim$ 580 nm [17], though the present optical arrangement (figure 1) only images the wavelength range 550 nm $< \lambda <$ 580 nm in order to ensure suppression of the illumination light.) Likewise, the emission intensity of SR101 displays a temperature dependence that varies with wavelength. In the case of ethanol as the solvent (figure 3(a)), this dependence is strongest at the lower wavelengths ($\lambda <$ 610 nm) while little temperature dependence is noted at the higher wavelengths ($\lambda >$ 610 nm) where the emission of SR101 is imaged in the present effort. It should also be noted that with ethanol as the solvent, the current filtering arrangement (figure 1) nearly eliminates the emission of RhB from camera β (the imaging device for the SR101 emission), while camera α (the imaging device for the RhB emission) captures a significant fraction of the SR101 emission. Therefore, equation (3) can be simplified to

$$\frac{I_A}{I_B} = \frac{V^\alpha - \Pi_B V^\beta}{V^\beta}, \tag{4}$$

where $\Pi_B(T) = V^\alpha_{C_A=0}(T)/V^\beta_{C_A=0}(T)$, represents the ratio of the emission from SR101 imaged by cameras α and β, respectively, when $C_{\mathrm{RhB}} = 0$. In contrast, with water as the solvent, the optics presented in figure 1 yield perfect separation of the fluorescent emissions (within the background noise levels of the cameras), meaning imaging of RhB and SR101 emissions by cameras β and α, respectively, need not be considered. Under these circumstances, the ratio of the separated emissions from both dyes acquired by cameras α and β is simply given by equation (2).

Figure 4 presents the normalized emission intensities of RhB and SR101, dissolved in water, acquired simultaneously using cameras α and β, respectively, when the dye mixture is illuminated using successive laser pulses. Each data point in figure 4 represents an average over a 30 × 30 pixel area (22.2 × 22.2 μm) in a single image associated with illumination by a single laser pulse. Additionally, for each illumination pulse, the ratio of the emissions from RhB and SR101 are computed and presented in figure 4. Measurements of the emissions from both dyes are acquired in the interior of a PDMS microchannel of width 1 mm through which the dye mixture is flowed by means of a syringe pump (Harvard Apparatus, PHD2000). Care is taken to ensure that the temperature of the dye mixture is kept constant at 20 °C using a circulating water bath. By performing the measurements in such a manner, it is ensured that the emissions from both dyes are not tainted by photobleaching effects and are minimally influenced by variations in the fluid temperature. Therefore, any variations in the emissions from both dyes are directly attributable to fluctuations in the illumination intensity of the incoming laser pulses. Figure 4 illustrates that the emissions from RhB and SR101 vary by roughly ±6% about the mean intensity between successive laser pulses. This degree of variability is quite consistent with the published

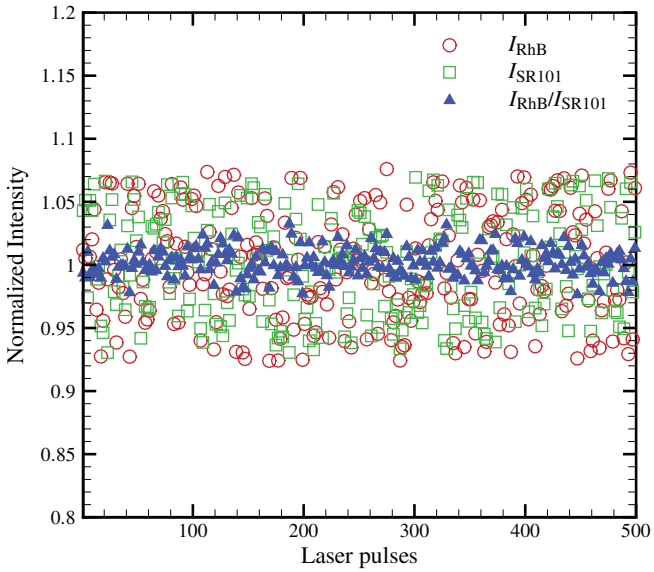

Figure 4. Variation of the fluorescence emission from the two dyes as a function of number of laser pulses used for illumination of the dyes. The dye solution is continuously flowing to avoid photobleaching effects.

energy stability of the Nd:YAG laser employed herein. In contrast, the intensity ratio of the simultaneous emission from both dyes exhibits a notable decrease in scatter about the mean of roughly ±1.5% which is likely associated with random noise in the CCD arrays as well as noise due to volume illumination. Therefore, figure 3 clearly illustrates the efficacy of the two-color LIF technique in compensating for the fluctuations in the incident illumination intensity from one laser pulse to another.

5. Results

5.1. Calibration

Figure 5 presents a schematic of the device used to calibrate the temperature dependence of the two dyes. A circular reservoir of diameter 20.0 mm and depth of 2.0 mm is filled with the dye solution and placed on an aluminum stage connected to a temperature-controlled water bath (TC-501, Brookfield). The side walls of the reservoir are insulated using silicon rubber and the top is covered by a 2.0 mm thick glass slide. The temperature of the dye solution inside the reservoir is monitored using a thermocouple (Type T, Quick-response PFA-Insulated Probes, Cole Palmer) and provides an independent measure of the fluid temperature within the reservoir. At a known temperature, when illuminated using an Nd:YAG laser pulsed at 1 Hz with 12 mJ of energy per pulse, the emission from the dye solution is imaged by the camera and an ensemble of ten successive images of the fluorescence emission is acquired. An average over the ensemble is performed in order to minimize the variations in the illuminating light. Following this, a spatial average over a region of 30 × 30 pixels is performed at each temperature in order to minimize variations in the noise from the CCD array. As such, the spatial domain over which the emission intensities

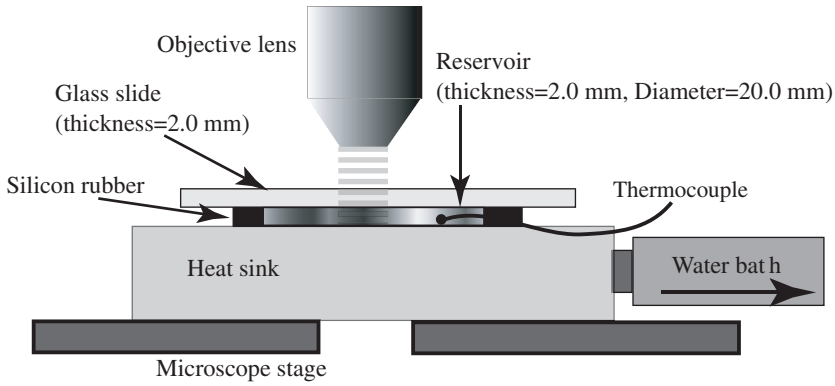

Figure 5. Schematic of the microfluidic device used to calibrate the temperature dependence of RhB and SR101.

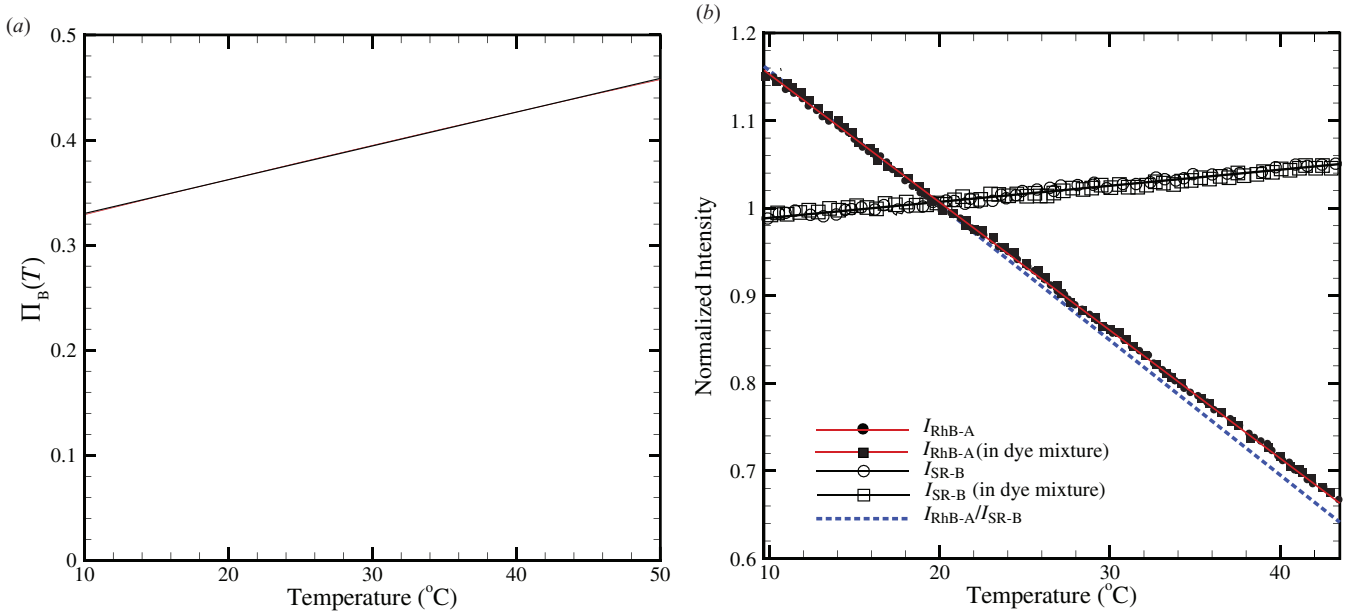

Figure 6. (a) Variation of Π_B, the ratio of the emission from SR101 dissolved in ethanol, imaged by cameras α and β, respectively, as a function of temperature. (b) Temperature dependence of the fluorescence emission of SR101 and RhB dissolved in ethanol. The measured intensities are normalized by the intensity at 20 °C (I_{20}).

are averaged provides a direct estimate of the spatial resolution of the measurement technique [12, 14]. For the current system, averaging over a spatial domain of 30 × 30 pixels limits the spatial resolution of the measurement technique to 22.2 × 22.2 μm and the resulting standard deviation of the residuals from the polynomial fit is calculated to be 0.4 °C. This procedure is repeated until image ensembles are acquired at several known temperatures spanning the range 10–60 °C. A single, average intensity value associated with each temperature is then obtained using the ensemble of the fluorescence emission acquired at that temperature.

As illustrated in equation (4), in order to obtain the variation of the intensity ratio, I_A/I_B, as a function of temperature for the dye mixture dissolved in ethanol, one must first obtain $\Pi_B(T)$ (the ratio of the emission from SR101 imaged by cameras α and β, respectively, when $C_{RhB} = 0$). Figure 6(a) presents the variation of Π_B as a function of temperature, obtained by imaging the emission from SR101 alone (concentration of 0.01 mg l^{-1} in ethanol) using both cameras α and β. The variation of Π_B with temperature is linear and increases at the rate of approximately +0.27% K^{-1}. Ideally, if the emission from SR101 over the range of wavelengths captured by cameras α and β showed nearly-identical temperature dependence, Π_B would be roughly constant over the entire range of temperature. Instead, the steady increase in the value of Π_B with increase in temperature is consistent with the trends of the emission spectra of SR101 in figure 3 which illustrate that the SR101 emission at lower wavelengths (acquired by camera α) exhibits a stronger temperature dependence compared to the SR101 emission at higher wavelengths (acquired by camera β).

Figure 6(b) presents the calibration curves of the fluorescence emission of RhB dissolved in ethanol (concentration of 0.005 mg l^{-1}) measured both separately and in the presence of SR101 as a part of the dye mixture, with all measured intensity values normalized by their corresponding intensity values at 20 °C. Additionally, the calibration curves of the SR101 emission, measured both separately and in the

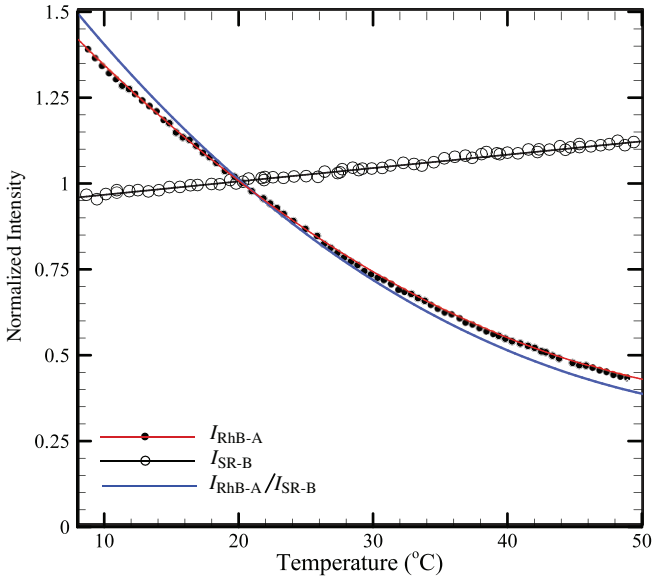

Figure 7. Temperature dependence of the fluorescence emission of SR101 and RhB dissolved in water. The measured intensities are normalized by the intensity at 20 °C (I_{20}).

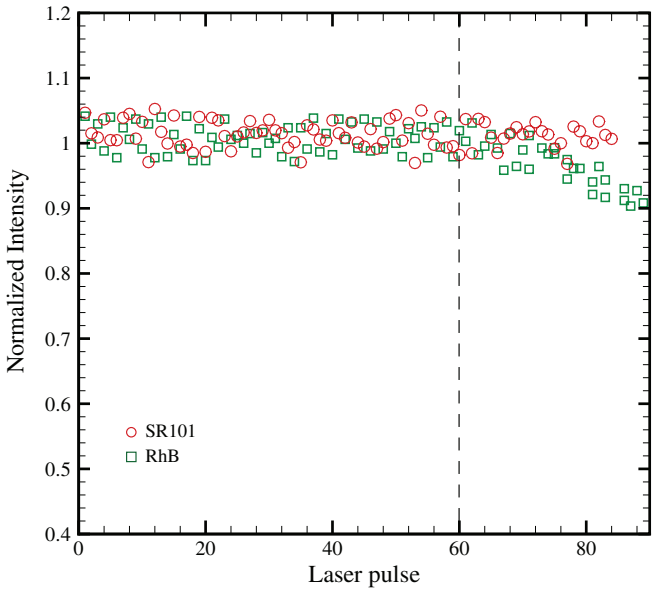

Figure 8. Variation of the emission intensity of RhB and SR101 as a function of number of laser pulses used for illumination of the dyes illustrating the onset of photobleaching in the case of RhB. The measured intensities are normalized by the mean intensity at 20 °C (I_{20}).

presence of RhB as a part of the dye mixture (the concentration of SR101 in both cases is 0.01 mg l^{-1}), are shown in figure 6(b). As expected, RhB displays a strong temperature dependence, with the fluorescence emission varying at a rate of approximately −1.45% K^{-1}. On the other hand, the calibration curves of SR101 indicate a slight increase in the emission intensity with temperature of approximately +0.14% K^{-1}—consistent with its rather weak temperature dependence at higher wavelengths (figure 3). With respect to the possibility of spectral conflicts associated with absorption of the emission from RhB by SR101 and vice-versa, the normalized calibration curves of the RhB emission evaluated both separately and in the presence of the SR101 as a part of the dye mixture collapse well. Likewise, the normalized calibration curves for SR101 acquired both separately and in the presence RhB as a part of the dye mixture show excellent consistency. These strong consistencies therefore support the notion that the simultaneous presence of RhB and SR101 has no measurable influence on their normalized fluorescence emissions as a function of temperature. These normalized intensity values, along with Π_B in figure 6(a), are used to compute the intensity ratio, I_{RhB}/I_{SR101}, at each temperature step using equation (4) which yields a calibration curve for the intensity ratio of the dye combination as a function of temperature. As illustrated in figure 6, the temperature sensitivity of the RhB–SR101 dye combination in ethanol is approximately −1.50% K^{-1}, slightly higher than the sensitivity of RhB alone. On the other hand, with water as the solvent, the fluorescence emissions of both RhB (concentration of 0.005 mg l^{-1}) and SR101 (concentration of 0.01 mg l^{-1}) show a stronger dependence on temperature (figure 7), with the fluorescence emissions varying at rates of approximately −2.6% K^{-1} and +0.38% K^{-1}, respectively. The resulting intensity ratio, I_{RhB}/I_{SR101}, calculated using equation (2) since perfect separation is achieved with water as the solvent (within measurable limits), reveals that the temperature sensitivity of RhB–SR101 dye combination in water is roughly −2.7% K^{-1}, notably higher than that obtained for the same dye combination in ethanol. This difference highlights the important role the solvent plays in the resulting temperature sensitivity of this technique.

Finally, it is important to note that prolonged exposure of fluorescent molecules to high-intensity incident light can eventually lead to their degradation, a phenomenon known as photobleaching. Photobleaching effects are irreversible and can severely compromise the accuracy of methods that rely upon quantitative measurements of fluorescence. In cases where such effects cannot be avoided, one can attempt to compensate for such losses by performing an *a priori* photobleaching calibration that embodies these effects. Figure 8 presents the intensity of RhB and SR101 (concentration of 0.005 mg l^{-1} and 0.01 mg l^{-1} in ethanol, respectively) as a function of the number of successive laser pulses used to illuminate the dyes. The temperature of the dyes is maintained at 20 °C using a circulating water bath. Therefore, any variations in the emission intensity of the dyes are directly attributable to variations in the incoming illumination and photobleaching effects. In figure 8, the emissions from SR101 and RhB exhibit fluctuations on the order of approximately 6% about the mean intensity between successive laser pulses. While the mean emission intensity of SR101 remains relatively constant for over eighty laser pulses, the mean emission from RhB decreases steadily after sixty laser pulses, indicating the onset of photobleaching effects in RhB (similar trends are noted with water as the solvent). These results therefore suggest that photobleaching effects can be minimized in the present system by limiting the exposure

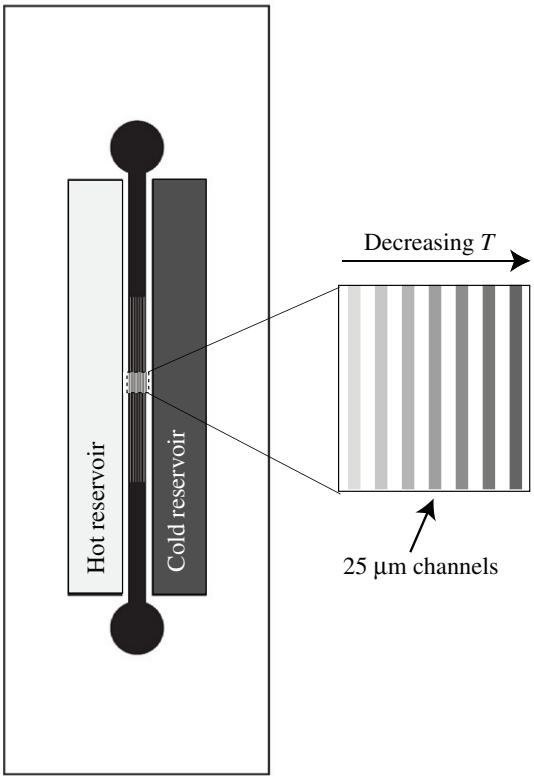

Figure 9. Schematic of the device utilized to obtain a one-dimensional, steady-state temperature gradient at the microscale.

of the same volume of the dye mixture to less than sixty laser pulses.

5.2. Temperature measurement

The two-color LIF technique described herein is implemented in the measurement of a one-dimensional, steady-state temperature gradient in a microfluidic device consisting a series of parallel microfluidic channels (similar to the device employed by Mao *et al* [18]). An array of seven parallel microchannels (width = 25 μm, depth = 100 μm; made of PDMS) spaced 175 μm apart are fabricated between two large reservoirs (width = 3.2 mm, depth = 3.2 mm) spaced 2 mm apart, that act as a heat source and heat sink, respectively (figure 9). Continuous circulation of heated and cooled water through the reservoirs ensures that they remain at constant temperatures. An independent measure of the temperature of the heated and cooled walls on either side of the channel array is obtained by inserting two thermocouples into the device through the hot and the cold reservoirs, respectively. As found by Mao *et al* [18], such an arrangement generates a linear temperature profile across the array of channels that are filled with the dye mixture. When illuminated with the Nd:YAG laser, a measure of the temperature of the dye mixture in each channel is obtained by imaging the fluorescence emission from the dyes.

Figures 10(a) and 10(b) present the variation of the steady-state temperature distribution across the microchannel array imposed by the hot and cold reservoirs obtained using the RhB–SR101 dye combination in ethanol and water, respectively. In order to conduct these measurements, the optical configuration illustrated in figure 1 is utilized for acquiring the emission from the dye mixture within the microchannels. For both systems, the emissions from RhB and SR101 are acquired simultaneously as image pairs using cameras α and β, respectively. Additionally, for the case of ethanol as the solvent (figure 10(a)), upon acquisition of each image pair, the emission imaged by both cameras is separated into its RhB and SR101 counterparts using equation (4). Finally, the ratio of the emission intensities of RhB and SR101 are computed for the intensity values recorded at each pixel location of the image and these intensity ratios are then converted to their corresponding temperature values using the calibration curves presented in figures 6 and 7. In both cases, acquisition of image pairs is limited to sixty (to avoid photobleaching effects as discussed above) upon the attainment of a steady-state temperature distribution across the hot and the cold reservoirs. As such, sixty statistically-independent measurements of the temperature distribution across the microfluidic device are obtained. Finally, consistent with the calibration methodology employed, averaging over a spatial domain of 30 × 30 pixels is performed which gives a spatial resolution for the LIF measurements of 22.2 × 22.2 μm. As such, since each microchannel is 25 μm wide, this averaging procedure simply yields the average fluid temperature within each microchannel.

In figures 10(a) and (b), the filled circles illustrate the mean temperatures of the dye mixture in the microchannel array obtained by averaging over the sixty LIF samples, while the predicted linear temperature variation across the device (presented as solid lines in figure (10)) is obtained by fitting a line through the independently-measured wall temperatures of the hot and the cold reservoirs for each of the two experiments. A measure of the uncertainty in the measurements is assessed by computing the standard deviation of the data sets comprising the ensemble. (Table 1 presents the mean and standard deviation for the temperature measurements in each of the seven microchannels of the microfluidic device contrasted with the linear prediction.) Figure 10(a) illustrates that the mean temperature of the dye mixture in each of the seven microchannels of the microfluidic device measured using the RhB–SR101 dye combination in ethanol is in good agreement with the predicted temperature distribution (span of error bars represent two standard deviations). As shown in table 1, the mean temperatures are within ± 0.4 °C of their predicted values with standard deviations of ±0.48–0.59 °C (with no discernable dependence on temperature). Likewise, very good agreement is observed between the measured values of the mean temperature in each of the seven channels and that predicted from the linear temperature profile (± 0.3 °C) for the measurement performed using the RhB–SR101 dye combination in water (figure 10(b)). The standard deviations of these measurements are in the range ±0.41–0.49 °C, slightly lower than that obtained for the measurements in ethanol. Alternatively, this variability can be recast into a relative uncertainty by normalizing the standard deviations by the measured temperatures. This normalization

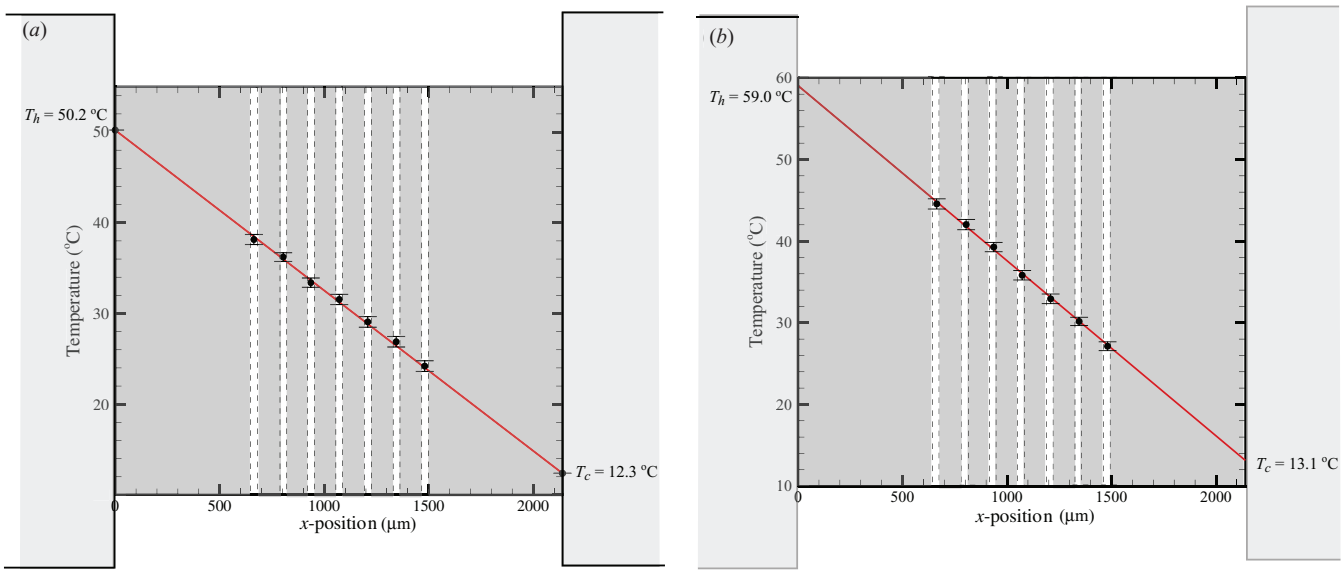

Figure 10. Variation of temperature across the microfluidic device shown in figure 9 measured using the RhB–SR101 dye combination dissolved in (a) ethanol and (b) water. The solid circles represent the mean temperatures obtained via two-color LIF measurements while the solid line indicates the predicted linear temperature profile across the channel array based on independent thermocouple measurements of the reservoir temperatures. The span of the error bars represents two standard deviations (see table 1).

Table 1. Temperature distribution across the channel array.

	x-coordinate (μm)	Measured temperature (°C)	Linear prediction (°C)	Standard deviation (°C)	Relative uncertainty (%)
	663	38.1	38.4	0.55	1.4
	804	36.2	35.9	0.48	1.4
	936	33.2	33.6	0.51	1.5
RhB–SR101	1072	31.5	31.3	0.56	1.5
in ethanol	1209	29.1	28.8	0.58	1.7
	1345	26.8	26.4	0.57	1.9
	1481	24.1	24.0	0.59	2.0
	663	44.9	45.1	0.44	1.0
	804	42.1	42.1	0.43	1.0
	936	38.9	39.2	0.41	1.1
RhB–SR101	1072	36.7	36.5	0.47	1.3
in water	1209	33.8	33.6	0.49	1.5
	1345	30.6	30.8	0.45	1.5
	1481	27.9	27.9	0.46	1.6

yields relative measurement uncertainties of 1.4–2% and 1–1.6% for the RhB–SR101 dye combination in ethanol and water, respectively, with the relative uncertainty increasing slightly with decreasing temperature. The lower absolute and relative uncertainties for the measurements with water as the solvent are attributable to the higher temperature sensitivity of the RhB–SR101 dye combination in water (-2.7% K^{-1}) compared to ethanol (-1.5% K^{-1}).

6. Summary and conclusions

The results presented herein demonstrate the suitability of two-color fluorescent thermometry for accurate measurement of fluid temperature at the microscale. Due to the short thermal-transport timescales that exist at the microscale, a pulsed Nd:YAG laser is employed as the illumination source. In particular, the experimental uncertainties associated with temperature measurements acquired by two-color LIF at the microscale are documented wherein errors associated with variability in the intensity of the illuminating light are minimized. Rhodamine B and Sulforhodamine-101 are employed as the temperature-sensitive and temperature-insensitive dyes respectively, and this dye combination yields temperature sensitivities of approximately -1.50% K^{-1} and -2.70% K^{-1}, when dissolved in ethanol and water, respectively. The capability of these systems in measuring fluid temperature at the microscale is demonstrated by conducting measurements of a one-dimensional steady-state temperature gradient across a microfluidic device consisting of seven parallel microfluidic channels. These measurements

reveal experimental uncertainties of ±0.48–0.59 °C and ±0.41–0.49 °C for the RhB–SR101 dye combination in ethanol and water, respectively, with a spatial resolution of $22.2 \times 22.2\ \mu$m. The relative uncertainties in the measurement of fluid temperature with the RhB–SR101 combination in water are 1–1.6%, which are lower than that observed using the same dye combination in ethanol (1.4–2%). This difference is attributable to the weaker temperature sensitivity of RhB in ethanol ($\approx -1.45\%\ \mathrm{K}^{-1}$) compared to water as the solvent ($\approx -2.6\%\ \mathrm{K}^{-1}$).

Finally, comparing the absolute uncertainties of $\sim\pm 0.55$ °C and $\sim\pm 0.45$ °C for the RhB–SR101 combination in ethanol and water, respectively, with the ±1.5 °C reported by Ross *et al* [12] for a single-dye, single-color volume-illumination microscale implementation indicates that a sizable portion of their error is likely due to variations in illumination intensity rather than volume illumination. Nevertheless, volume illumination plays a non-trivial role in microscale fluorescent thermometry as the uncertainties reported herein are still 2–3 times larger than those reported for macroscale, two-dye LIF [7, 8].

Acknowledgments

This work is supported by the Air Force Office of Scientific Research under grant FA9550-05-1-0346 (Drs Les Lee and Hugh DeLong, Program Managers).

References

[1] Kandlikar S G 2003 Microchannels and minichannels–history, terminology, classification and current research needs *Proc. 1st Int. Conf. on Microchannels and Minichannels* pp 1–6

[2] Lu G Q and Wang C Y 2005 Development of micro direct methanol fuel cells for high power applications *J. Power Sources* **144** 141–5

[3] Dittrich P S and Manz A 2006 Lab-on-a-chip: Microfluidics in drug discovery *Nat. Rev. Drug Discovery* **5** 210–8

[4] Erickson D and Li D 2004 Integrated microfluidic devices *Anal. Chim. Acta* **505** 11–26

[5] Wu S, Mui J, Tai Y C and Ho C M 1999 Micro heat exchanger by using MEMS impinging jets *Proc. IEEE Micro Electro Mechanical Systems* pp 171–6

[6] Sakakibara J, Hishida K and Maeda M 1997 Vortex structure and heat transfer in the stagnation region of an impinging plane jet (simultaneous measurement of velocity and temperature fields by DPIV and LIF) *Int. J. Heat Mass Transfer* **40** 3163–76

[7] Sakakibara J and Adrian R J 1999 Whole field measurement of temperature in water using two-color laser induced fluorescence *Exp. Fluids* **26** 7–15

[8] Sakakibara J and Adrian R J 2004 Measurement of temperature field of Rayleigh-Bénard convection using two-color laser-induced fluorescence *Exp. Fluids* **37** 331–40

[9] Funatani S, Fujisawa N and Ikeda H 2004 Simultaneous measurement of temperature and velocity using two-colour LIF combined with PIV with a colour CCD camera and its application to the turbulent buoyant plume *Meas. Sci. Technol.* **15** 983–90

[10] Lavieille P, Lemoine F, Lavergne G and Lebouché M 2001 Evaporating and combusting droplet temperature measurements using two-color laser-induced fluorescence *Exp. Fluids* **31** 45–55

[11] Bruchhausen M, Guillard F and Lemoine F 2005 Instantaneous measurement of two-dimensional temperature distributions by means of two-color planar laser induced fluorescence (PLIF) *Exp. Fluids* **38** 123–31

[12] Ross D, Gaitan M and Locascio L E 2001 Temperature measurement in microfluidic systems using a temperature-dependent fluorescent dye *Anal. Chem.* **17** 4117–23

[13] Yoon S Y and Kim K C 2006 Signal intensity enhancement of μ-LIF by using ultra-thin laser sheet illumination and aqueous mixture with ethanol/methanol for micro-channel applications *Opt. Lasers Eng.* **44** 224–39

[14] Kim H J, Kihm D K and Allen J S 2003 Examination of ratiometric laser induced fluorescence thermometry for microscale spatial measurement resolution *Int. J. Heat Mass Transfer* **46** 3967–74

[15] Soloff S M, Adrian R J and Liu Z C 1997 Distortion compensation for generalized stereoscopic particle image velocimetry *Meas. Sci. Technol.* **8** 1441–54

[16] Copetta J and Rogers C 1998 Dual emission laser induced fluorescence for direct planar scalar behavior measurements *Exp. Fluids* **25** 1–15

[17] Lavieille P, Delconte A, Blondel D, Lebouché M and Lemoine F 2004 Non-intrusive temperature measurements using three-color laser-induced fluorescence *Exp. Fluids* **36** 706–16

[18] Mao H, Yang T and Cremer P S 2002 A microfluidic device with a linear temperature gradient for parallel and combinatorial measurements *J. Am. Chem. Soc.* **124** 4432–5